# Experimental characterization of anomalous strong scattering of mm-waves in TEXTOR plasmas with rotating islands

**S. K. Nielsen[1], M. Salewski[1], E. Westerhof[2], W. Bongers[2], S. B. Korsholm[1], F. Leipold[1], J. W. Oosterbeek[3], D. Moseev[2], M. Stejner[1] and the TEXTOR team[4]**

[1] Association EURATOM - DTU, Dept. of Physics, Technical University of Denmark, Risoe Campus, DK-4000 Roskilde, Denmark

[2] FOM Institute DIFFER, Dutch Institute for Fundamental Energy Research, Association EURATOM - FOM, Nieuwegein, The Netherlands

[3] Eindhoven Univ. Technol., Dept. Mech. Engn., Control Syst. Technol Grp., NL-5600 MB Eindhoven, Netherlands

[4] Forschungszentrum Jülich GmbH, Institute of Energy Research, Plasma Physics, Association EURATOM-FZJ, Trilateral Euregio Cluster, 52425 Jülich, Germany

**Abstract.** Anomalous scattering of high power millimetre waves from gyrotrons at 140 and 110 GHz is investigated for plasma with rotating islands at TEXTOR. The magnetic field and plasma density influence the spectral content of the scattered waves and their power levels significantly. Anomalous strong scattering occurs in two density regimes, a low-density and high density regime, that also depend on magnetic field. The two regimes are separated by a quiescent regime without anomalous scattering. Investigations suggest that scattering in the high-density regime is generated at the low-field side intersection of the gyrotron beam and the island position. The transition from the quiescent regime to the high-density regime occurs when the gyrotron frequency is twice the upper hybrid frequency at this position. There is some evidence that the scattering in the low-density regime is generated near the plasma centre. Under this assumption all the observed scattering is generated when the gyrotron frequency is near or below twice the upper hybrid frequency.

## 1. Introduction

Millimetre waves are frequently used in tokamak plasmas for electron heating, current drive, and diagnostic purposes [1,2]. Electron cyclotron resonance heating (ECRH) and electron cyclotron current drive (ECCD) by millimetre waves generated in gyrotrons are well established schemes for tokamaks as well as stellerators. For ECRH and ECCD it is important that the launched power is absorbed and transferred to the plasma at a pre-determined position. It is crucial that the millimetre waves do not drive instabilities before the power is deposited in the plasma. From a diagnostic point of view, a decay of the millimetre waves will increase the requirement for protection of millimetre wave

diagnostics and will hamper electron cyclotron emission (ECE) based NTM control systems [3–5] and diagnostics such as collective Thomson scattering (CTS) [6–9].

In the parametric decay instability (PDI), the radiation is split up into two daughter waves when the incident power level is above a given threshold for specific plasma parameters [10, 11]. This has been observed in laboratory and astrophysical plasmas [12–14]. PDI has previously been observed during ECRH in the Versator II tokamak [15] where millimetre waves from a gyrotron with a frequency of 35 GHz decayed at the upper hybrid frequency into a lower hybrid wave and an electron Bernstein wave. The power threshold was measured to 50 kW which is similar to theoretical predictions for inhomogeneous plasmas [15]. In recent results from TEXTOR [16, 17] strong scattering signals were seen during ECRH when rotating islands were present in the plasma. The observations have been suggested to originate from parametric decay even though the gyrotron frequency was far from the upper hybrid frequency. The TEXTOR results have motivated a re-evaluation of the parametric decay power threshold [18–22].

At TEXTOR, when rotating islands are present in the plasma, anomalous scattering is observed in two different regimes: a low-density regime and a high-density regime. The two regimes are separated by a quiescent regime at intermediate densities with no noticeable anomalous scattering. In the high-density regime the anomalous scattering is strongly correlated to the passage of the island O-point through the ECRH beam. In this regime, we have previously reported experiments with varying receiver beam geometry which indicate that the scattering originates from the intersection of the island position and the gyrotron beam [17]. This type of scattering is only observed in the presence of magnetic islands. Our experiments suggest that the anomalous spectra in the high-density regime are not caused by spurious modes in the gyrotron cavity. The anomalous scattering in the high-density regime is observed when the gyrotron frequency is equal to or slightly below twice the upper hybrid frequency at the low-field side island position. In the low-density regime the scattering signals are weakly modulated by the rotating island, and the frequency differences between the frequencies of the anomalous scattering signals and of the gyrotron match the lower hybrid frequency (LH) in the plasma centre and harmonics thereof. This suggests that the scattering in the low-density regime is generated near the plasma centre. Under certain circumstances scattering similar to the signals observed in the low-density regime is also observed in plasmas without rotating magnetic islands. Here we focus on the scattering signals obtained in the presence of rotating magnetic islands. Under the assumption that the anomalous scattering in the low-density regime originates from the plasma centre, the anomalous scattering in both the high-density regime and the low-density regime occurs when the gyrotron frequency is near or just below twice the upper hybrid frequency.

The article is organised in the following way. In section 2 we briefly review the experimental set-up in which a 140 GHz gyrotron is used for heating and current drive. We show a strong dependence of the anomalous scattering on the electron density and the magnetic field. The high-density regime of strong scattering is separated from the low-density regime of strong scattering by an intermediate-density quiescent regime in

which no strong scattering is detected. This is illustrated in section 3. In section 4 the low-density regime is discussed and in section 5 we focus on the high-density regime and reveal fine-grained frequency structure of the scattering signals. In section 6 we study the dependence of strong scattering in the high-density regime on the scattering geometry. In section 7 we demonstrate that strong scattering occurs likewise at a gyrotron frequency of 110 GHz. We show that a qualitatively different type of strong scattering occurs if the plasma is placed between the first and second harmonic resonances, as for CTS experiments at TEXTOR or ASDEX Upgrade [6, 8, 23]. We discuss our results and relate them to previous work in section 8 and conclude in section 9.

## 2. Experimental setup

The experiments reported in this article are performed on the TEXTOR tokamak (1.75 m major radius, minor radius 0.45 m) [24]. The dynamic ergodic divertor (DED) [25] is used to create a rotating m/n = 2/1 islands by applying an AC current with a frequency of 974 Hz [26]. In the discharges dedicated to study the anomalous scattering, co-current neutral beam injection was applied at a power of 0.3 MW to facilitate triggering the mode. The mode locks to the rotating field created by the DED which allows us to study the anomalous scattering in a controlled manner. The anomalous scattering signals also appear in discharges without neutral beam injection and with freely rotating islands without the use of DED. The island is detected by magnetic coils and by standard ECE diagnostics.

TEXTOR was at the time of the experiments equipped with two gyrotrons [27]; a gyrotron with a frequency of 140 GHz ($P_{gyr} \leq$ 1MW for 10s) used for plasma heating and a second gyrotron operating at 110 GHz ($P_{gyr} \leq$ 250kW for 200 ms) normally used for CTS experiments [17, 23]. Both gyrotrons at TEXTOR have been decommissioned. In the majority of the experiments we report, the 140 GHz gyrotron has been used for 2nd harmonic X-mode ECRH. During the operation of the gyrotron, large signals have been observed by two independent receivers within a frequency range in the order of 1-4 GHz from the gyrotron frequency: an in-line receiver sharing the transmission line with the gyrotron [4, 28] and a modified version of the CTS receiver [17].

The CTS receiver is the main diagnostic used in this article. This modified CTS receiver consists of 42 frequency channels spanning from 134.5 GHz to 141.5 GHz. Notch filters are used to attenuate the gyrotron frequency around 140 GHz. In the vicinity of 138.5 GHz, the receiver has a frequency resolution of 80 MHz and the time resolution is 10 $\mu$s. The plasma facing mirror of the receiver transmission line is located around 20 cm above the gyrotron launcher mirror and is steerable during a plasma discharge. Thus a variety of scattering geometries can be realized with this setup. An example of a possible scattering geometry is shown in figure 1. In this specific configuration the beam patterns of the CTS receiver and of the gyrotron overlap at about R = 2.0 m which is close to the position of the rotating island induced by the DED coils. A detailed

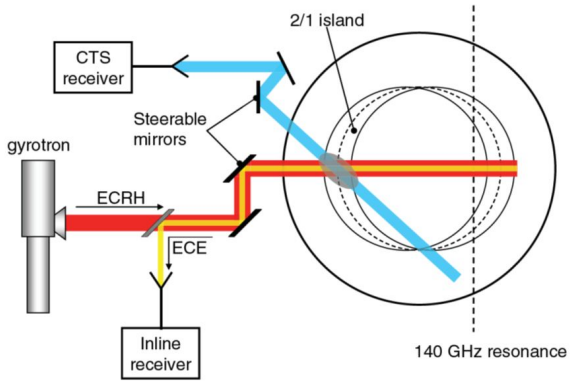


**Figure 1.** Schematic of the experimental setup (also published in [16]). The gyrotron and both the inline-ECE and CTS diagnostics view the plasma (solid circle) from the low-field side. The gray oval at the intersection of ECRH and CTS beams indicates the CTS scattering region. Backscattered radiation along the inline-ECE view can come from the entire ECRH beam path in the plasma up to the resonance where the power is absorbed.

description of the diagnostic can be found in reference [17].

## 3. Overview of anomalous scattering regimes

The time traces of the main plasma parameters for a typical discharge used to investigate the anomalous scattering in plasmas with rotating islands are shown in figure 2. Neutral beam injection is applied at the end of the current ramp at $t = 1$ s, and the amplitude of the alternating DED current is slowly increased from $t = 1.5$ s to $t = 2.0$ s. An island is triggered during the DED current ramp at about $t = 1.8$ s, as can be seen by the decrease in the electron temperature at a radius of 2.0 m. From $t = 2.0$ s to 4.2 s ECRH is applied, and in this time window the central line-averaged electron density is slowly increased from 1.5 to $3.6 \times 10^{19}$ m$^{-3}$. During the density ramp the electron temperature at the island position decreases slowly from 0.8 kev to 0.6 keV.

A number of discharges have been performed with a fixed scattering geometry where the ECRH power, the plasma density and the toroidal magnetic field have been varied. The discharges are listed in table 1 specifying the following parameters: (1) the line-averaged density at the transition from the quiescent regime to the high-density regime measured by interferometry, (2) the local density in the vicinity of the island on the low-field side at the transition inferred from multi-channel interferometry [29], (3) the electron temperature at the transition obtained by electron cyclotron emission measurements [30], (4) the magnetic field at the position of scattering volume, (5) the plasma current, and (6) the gyrotron output power. The magnetic field was kept constant in each of the discharges whereas the line-averaged density was ramped slowly from 1.5 to $3.6 \times 10^{19}$ m$^{-3}$ except in discharges #108096 and #108100 where the ramp started at a line-averaged density of $2.1 \times 10^{19}$ m$^{-3}$. The plasma current was chosen to keep the island at the same position at the different magnetic fields. As illustrated

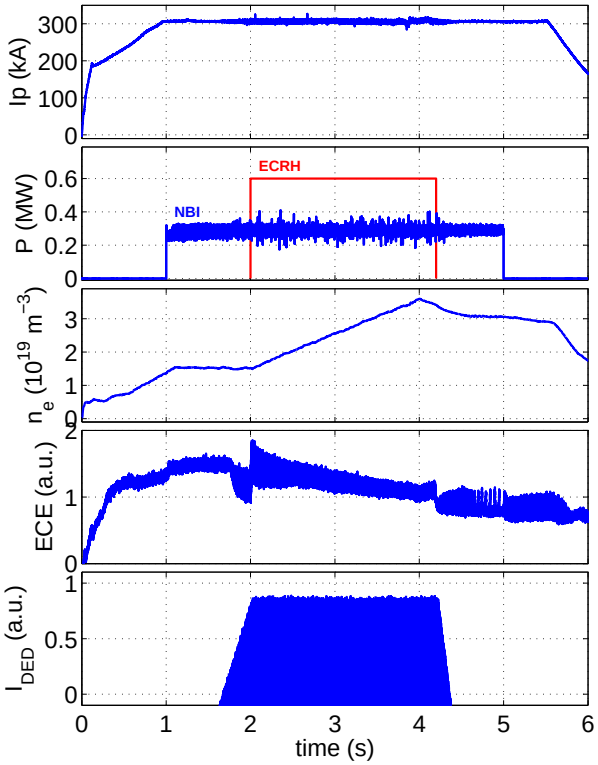


**Figure 2.** Time traces of main plasma parameters for TEXTOR discharge 108115. From top to bottom we show plasma current, neutral beam injected power (blue) and ECRH power (red), central line-averaged electron density, a standard ECE measurement at 109 GHz originating from close to the q = 2 surface on the low-field side, and DED current (AC).

**Table 1.** Overview of discharges with fixed scattering volume at 2.0 m and values at the transition from the quiescent regime to the high-density regime. From left to right: line-averaged density, electron density at the island position, electron temperature at the island position, on-axis magnetic field/magnetic field at the island position, plasma current, and ECRH power.

| Shot | $n_{eLA}$ ($10^{19}$m$^{-3}$) | $n_e$@ 2.01 m ($10^{19}$m$^{-3}$) | $T_e$@2.0 m (eV) | $B_T$@1.75 m / 2.0 m (T) | $I_p$ (kA) | $P_{gyr}$ (kW) |
|---|---|---|---|---|---|---|
| 108096 | 2.70 | 2.80 | 304 | 2.1 / 1.84 | 285 | 400 |
| 108099 | 1.71 | 1.89 | N.A. | 2.4 / 2.1 | 325 | 400 |
| 108100 | N.A. | N.A. | N.A. | 2.6 / 2.28 | 355 | 400 |
| 108111 | 2.31 | 2.40 | 591 | 2.25 / 1.97 | 305 | 200 |
| 108114 | 2.28 | 2.34 | 653 | 2.25 / 1.97 | 305 | 400 |
| 108115 | 2.28 | 2.32 | 699 | 2.25 / 1.97 | 305 | 600 |

in figure 3, the ECRH changes from central heating to high field side heating for these different magnetic fields. However, in all cases the ECRH and the receiver beams cross the island position on the low-field side. The toroidal injection angle was for these discharges $-4°$ from exactly perpendicular injection.

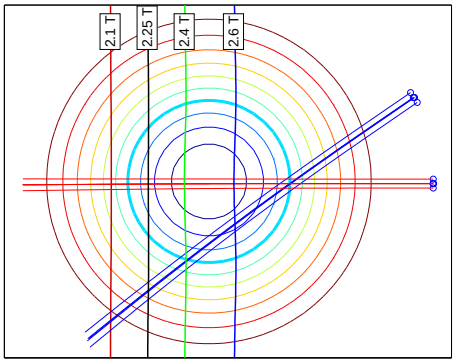


**Figure 3.** Tokamak cross section, beam patterns and the 140 GHz cold second harmonic resonance layer for an on-axis magnetic field of 2.1 T, 2.25 T, 2.4 T, and 2.6 T (vertical lines). The circles represent a contour plot of the flux function, $\psi$, with $\psi = 1$ at the outer most circle and $\psi = 0.1$ at the inner most circle. The thick circle indicates the island position. The horizontal lines represent the gyrotron beam pattern and the diagonal lines represent the CTS receiver beam pattern. The gyrotron is launched from the low-field side (tiny circles).

When ramping up the plasma density for a constant plasma current, magnetic field and DED current pattern, the characteristics of the observed anomalous scattering can generally be divided into three regimes. These regimes of strong scattering have been discussed in previous work [16] in terms of 10 ms averaging for individual frequency channels. In figure 4 we show the measured spectral power density for three different ECRH power levels. The averaging time interval was set to 1 ms to display the large-scale power dependence of strong scattering. In this view three seemingly different regimes of strong scattering appeared: one at low densities (label 1 in figure 4), followed by an intermediate-density quiescent regime where no significant anomalous scattering occurs (label 2 in figure 4), and a high-density regime (label 3 in figure 4). In the following sections we discuss the characteristics of these individual regimes.

The low-density regime of strong scattering is separated from the high-density regime by a quiescent regime at intermediate densities. This silent regime is limited by the upper and lower threshold densities at which anomalous scattering resumes. The upper as well as the lower threshold densities become lower when the magnetic field is increased. Figure 5 gives the functional dependence of the upper and lower density thresholds on the magnetic field. The quiescent regime takes the form of a corridor in the $B - n_e$-plane. Strong scattering occurs in regimes 1 and 3, but rarely in regime 2. In regime 2 scattering is only observed at a gyrotron power of 600 kW where a signal is present just outside the notch filter at about 139.5 GHz (see figure 4c label 2).

The upper hybrid frequency $f_{UH} = \sqrt{f_{pe}^2 + f_{ce}^2}$ depends on the magnetic field and the density. In figure 6 we plot the upper hybrid frequency at the low-field side island position for the four on-axis magnetic fields we used as function of local density using the local magnetic field. We also plot the upper and lower density thresholds of the quiescent regime measured at R=2.0 m. We note that at the upper density threshold the

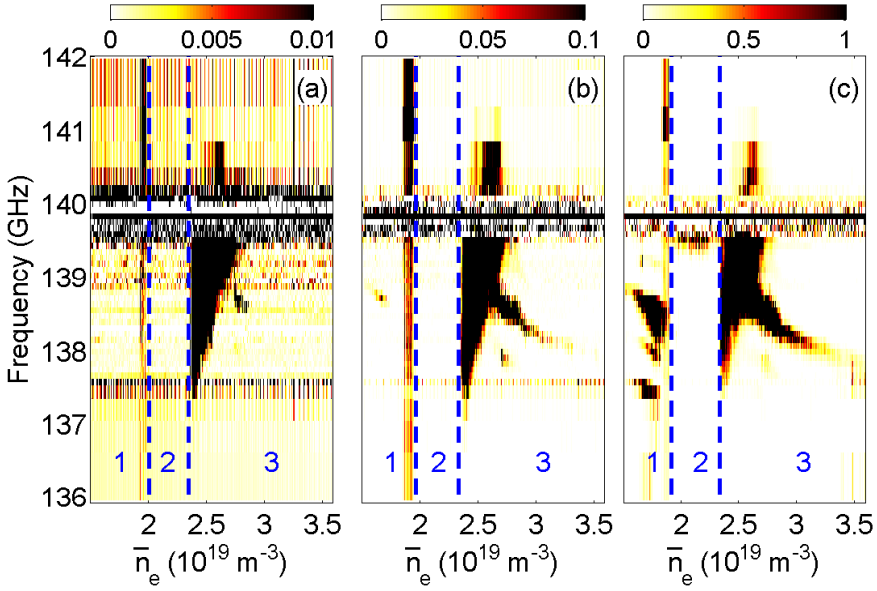


**Figure 4.** Measured spectrum (in MeV), averaged over 1 ms time windows, as a function of line-averaged electron density for three gyrotron power levels: 200 kW (a), 400 kW (b), and 600 kW (c), discharge 108111, 108114, and 108115, respectively. The transition densities between the low-density regime (1), the quiescent regime (2) and the high-density regime (3) are listed in table 1. The on-axis magnetic field is 2.25 T in these discharges. We note that the signal mainly has frequencies below the gyrotron frequency but signal above the gyrotron frequency (140 GHz) is also observed at the three power levels. In (a) the signal around 137.5 and 142 GHz is caused by receiver noise.

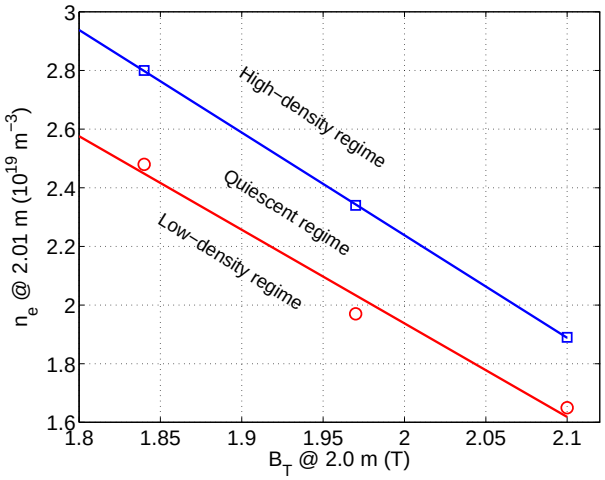


**Figure 5.** The transition values from the low-density regime to the quiescent regime and from the quiescent regime to the high-density regime are plotted as squares and circles, respectively, in an ($B_T$, $n_e$)-diagram. A straight line has been fitted to the transition points for illustration purposes.

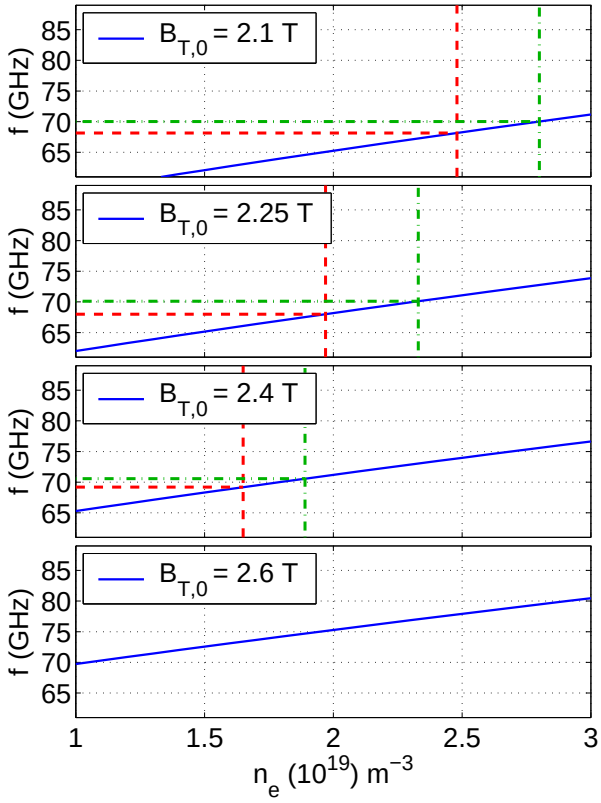


**Figure 6.** The upper hybrid frequency (solid line) at the low-field side island position as a function of density for a central magnetic field of (from top to bottom) 2.1T, 2.25T, 2.4T and 2.6T. The densities at the low-field side island position which are associated with the beginning (vertical dashed line) and end (vertical dash-dotted line) of the quiescent regime are indicated for each magnetic field.

upper hybrid frequency is close to 70 GHz corresponding to half the gyrotron frequency. Strong scattering only occurs when the upper hybrid frequency at the low-field side island position is larger than half the gyrotron frequency. In the discharge with a on-axis magnetic field of 2.6 T, no strong scattering was observed. Here, the local density at the low-field side island position was ramped up from $2.1 \times 10^{19}$ m$^{-3}$. Thus the upper hybrid frequency was always significantly larger than half of the gyrotron frequency as shown in the bottom panel of figure 6. The simultaneous occurrence of the upper density threshold with the crossing of the upper hybrid and half the gyrotron frequency has been argued to be due to two-plasmon instability [21, 31].

## 4. Anomalous scattering signals at low densities

In most of the discharges, the density scans were started at a line-averaged density of $1.5 \times 10^{19}$ m$^{-3}$. In the low-density regime, indicated by label 1 in figure 4, two distinct periods are identified. This is further illustrated in figure 7 which is a zoom of figure 4 at the densities corresponding to the low-density regime. In the first part of the density ramp a few well defined frequencies, the first four harmonics of the central lower

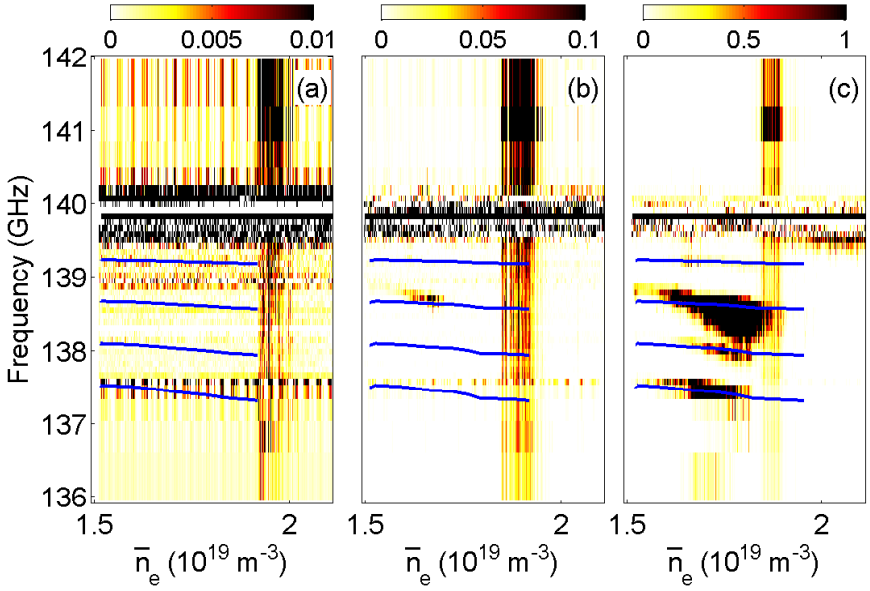


**Figure 7.** Zoom of figure 4 in the low-density regime. The evolution of the first four harmonics of the lower hybrid frequency are presented as solid blue lines.

hybrid frequency, $f_{LH} = \sqrt{(f_{ce}f_{ci})/(1 + f_{ce}^2/f_{pe}^2)}$, were identified in the $P_{gyr} = 600$ kW case displayed in figure 7c. This is further described in reference [17]. The signals are weakly modulated by the island rotation frequency and depend on the gyrotron power in a strongly non-linear manner. In the 400 kW case, only the second harmonic of $f_{LH}$ appears at a signal level several orders of magnitudes below the signal level in the 600 kW case. No anomalous scattering in the first part of the low-density regime can be identified for a gyrotron power of 200 kW. The signals below a line-averaged density of $1.8 \times 10^{19}$ m$^{-3}$ in figure 7(a) represent receiver noise.

The low-density regime is, for all three gyrotron power levels, terminated by bursts of anomalous scattering covering all channels in the CTS receiver. The signal intensity is largest at frequencies above the gyrotron frequency around 141 GHz. The individual bursts are strongly correlated with the passage of the O-point of the rotating island through the ECRH beam which is illustrated in figure 8. The passage time of the O-point is calculated based on the applied DED currents. The power levels of these signals also depend non-linearly on the gyrotron power, but not as strongly as the first part of the low-density regime. The densities at which the bursts are measured are similar for the different gyrotron power levels. The density region is slightly shifted to higher values for lower gyrotron power but this trend is within the error bars of the measured densities.

The spectral evolution during the bursting periods of the low-density regime, displayed in figure 8b, is similar for the different magnetic field and plasma current configurations listed in table 1. The main difference is the density at which they happen as was discussed in the previous section.

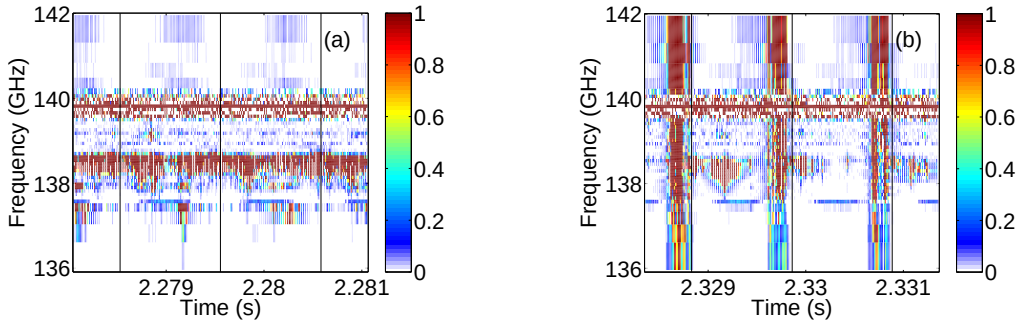


**Figure 8.** Spectral evolution (in MeV) during individual island passages in discharge 108115 ($B_T$ = 2.25 T, $P_{gyr}$ = 600 kW) during the non-bursting period at a line-averaged density of $1.79 \times 10^{19}$ m$^{-3}$ (left) and during a bursty period at line-averaged density of $1.85 \times 10^{19}$ m$^{-3}$ (right) in the low-density regime. The estimated island passage times are denoted by vertical lines.

## 5. Fine structure of anomalous scattering signals at high densities

At the onset of the high density regime the strong scattering stretches uninterrupted from the gyrotron frequency to a lower frequency level. At higher densities, no strong scattering is observed immediately below the gyrotron frequency but appears at increasing lower frequencies as the density is increased (see figure 4). These structures appearing in sliding averages are presented in figure 4 for different levels of gyrotron power. Qualitatively these structures are similar for the different gyrotron power levels. The spectral power density, however, can vary by orders of magnitude. One may note that the chirping structure in the sliding averages occurs at larger frequency shift for larger gyrotron power and that the spectral power density of that structure increases also non-linearly with gyrotron power.

Here we investigate the detailed structure of these last two phases and show that in fact similar underlying fine-grained structure can be found throughout the high-density regime of strong scattering. Figure 9 shows spectra acquired over the time period of an island passage for different densities. As identified previously [16], the strong scattering phenomenon occurs at several characteristic frequencies that chirp up and down when the O-point of the island passes the gyrotron beam as figures 9c and 9d illustrate. At densities just above the threshold for the high-density regime (figure 9a) the anomalous scattering is concentrated at the time of the island passage and extends from the gyrotron frequency down to 137.5 GHz with a maximum at around 138.5 GHz. The signal is only present shortly at the time close to the island passage. Structures in the signals are not resolved due to insufficient time resolution.

As the density is increased, the time fraction in which the signal is present increases, and structures start to emerge as shown in figure 9b. Typically, chirping is observed with the frequency decreasing continuously in the first half of the island passage from the gyrotron frequency to one or several discrete frequencies. The frequency change is

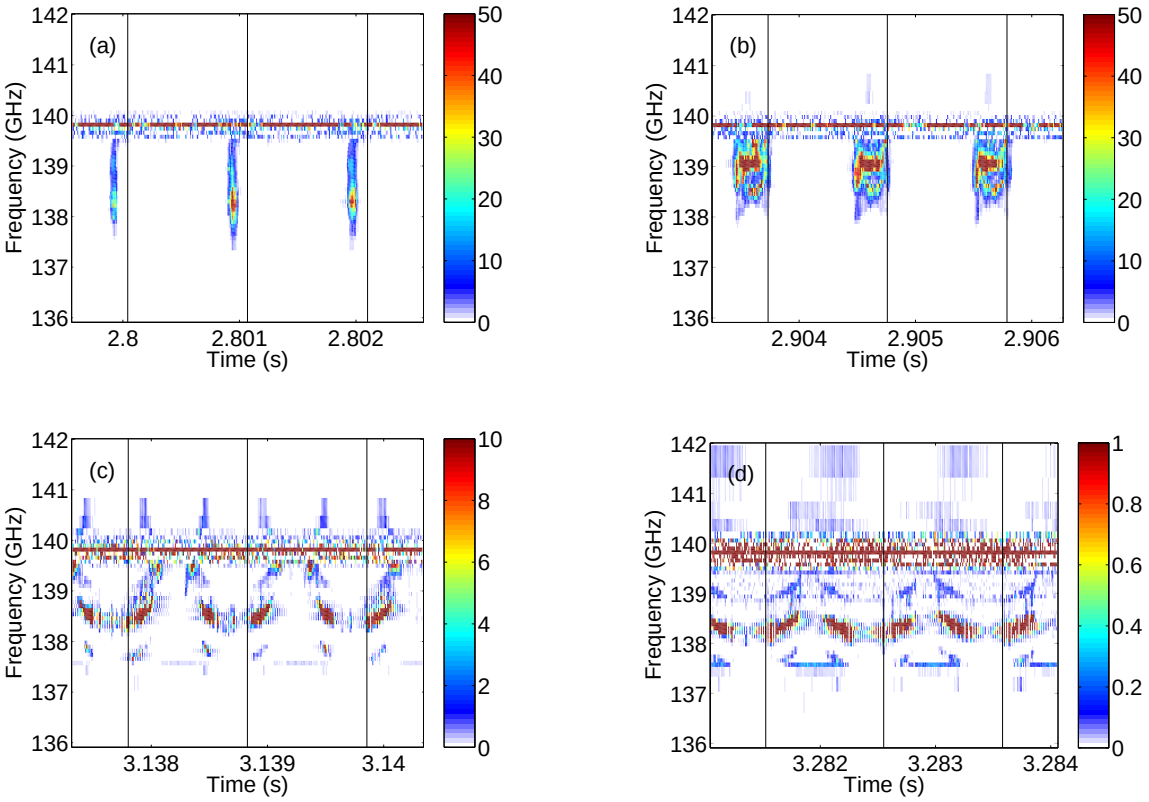


**Figure 9.** Spectral evolution (in MeV) during individual island passages in discharge #108115 ($B_T$ = 2.25 T) at line-averaged densities of (a) $2.34 \times 10^{19}$ m$^{-3}$, (b) $2.46 \times 10^{19}$ m$^{-3}$, (c) $2.68 \times 10^{19}$ m$^{-3}$, and (d) $2.83 \times 10^{19}$ m$^{-3}$. The estimated island passage times are denoted by vertical lines. The signal at 137.6 GHz in figure (c) and (d) is unreliable as this channel is noisy.

reversed in the second half of the island passage. As the density is further increased, the structures gradually evolve and the discrete frequencies become more obvious as shown in figure 9c. The power level of the scattering is decreased (note the change in colour scale). Three chirping lines are identified in the first half of the island cycle from 139.4 to 139.1 GHz, from 138.8 to 138.2 GHz, and from 138.0 to 137.6 GHz. As the density grows, the signal level is reduced to a level where it is finally not detectable by the receiver. The decrease of the signal level is illustrated in figure 9d. Here the chirp rate of the lines is significantly reduced. However, the signal is present during almost the entire island cycle and at the O-mode passage time the signal amplitude is reduced to below the detection limit. For higher densities, which are not shown here, the frequency of the discrete lines changes and the amplitude is slowly decreased until the lines are finally not detectable.

In figure 10 we capture the longer scale time-development of these fine-grained structures by plotting the lowest frequency reached at the end or at the start of the chirps for each of the discrete lines discussed above. As in figure 4 we show the development for the three gyrotron power levels. This reveals a line at a characteristic frequency

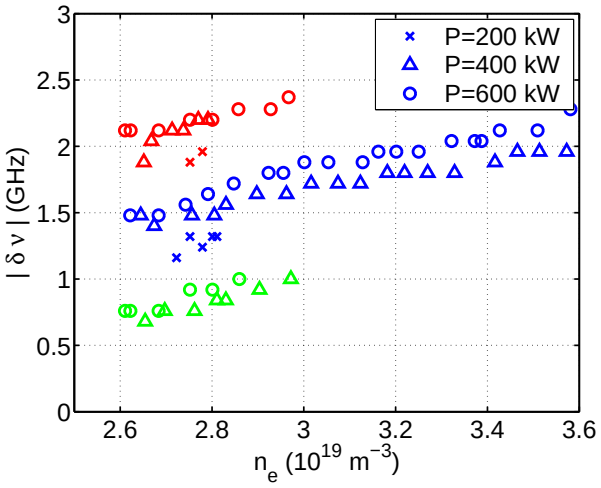


**Figure 10.** Development of characteristic frequencies during an individual island passage (see figures 9c and 9d) as a function of line-averaged density for the high density regime.

depending on the density that continues throughout the high-density regime (line at 138.2 GHz in figure 9c). The other characteristic frequencies which are shown in figure 9c occur only at the lower density part of the high-density regimes. We generally see that the frequency shifts are similar for each gyrotron power. The frequency shifts are slightly larger for larger gyrotron power because the lines are visible for longer periods of an island passage. For the low power level only two discrete frequencies are observed in a very narrow density region, whereas the other two power levels show similar frequency shifts as a function of density.

The dependence of the anomalous scattering has also been investigated for different magnetic fields. Figure 11 shows measured spectral power densities for three different magnetic fields. The averaging time interval was set to 1 ms to display the large-scale power dependence of strong scattering as in figure 4. The power level of the anomalous scattering is comparable at the three different magnetic fields. The scattering level slightly increases as the magnetic field goes up. However, the frequency coverage of the anomalous scattering also changes as the magnetic field is varied. In the beginning of the high-density regime at a magnetic field of 2.1 T anomalous scattering reaches frequencies down to 137 GHz, whereas only frequencies above 138 GHz are reached at 2.4 T.

The dependence of the fine-grained strong scattering structure on the magnetic field is shown in figure 12. Qualitatively similar structures occur at on-axis magnetic fields from 1.9 T to 2.4 T. In the discharge with an on-axis magnetic field of 2.6 T no strong scattering was observed. The lower hybrid frequency at the low-field side island position, which is also shown in the figures, does not match the observed frequency exactly. Both the observed frequency and the calculated lower hybrid frequency increases when the density is increased. The possible evolution of the island during the density scan is not measured and this effect is not included in the calculations.

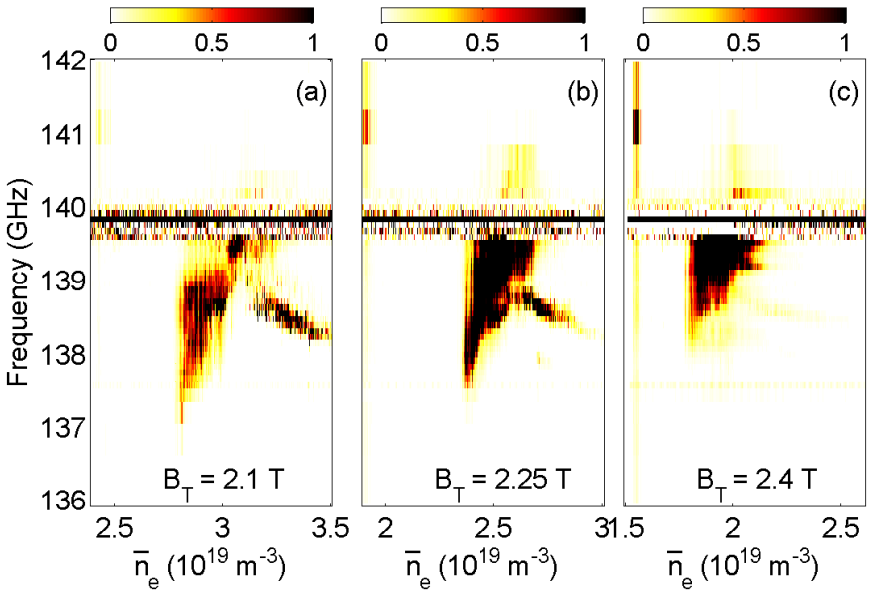


**Figure 11.** Measured spectral power densities (in MeV), averaged over 1 ms time windows, as a function of line-averaged electron density for different magnetic fields: $B_T = 2.1$ T (a), $B_T = 2.25$ T (b), and $B_T = 2.4$ T (c), discharge 108096, 108114, and 108099, respectively.

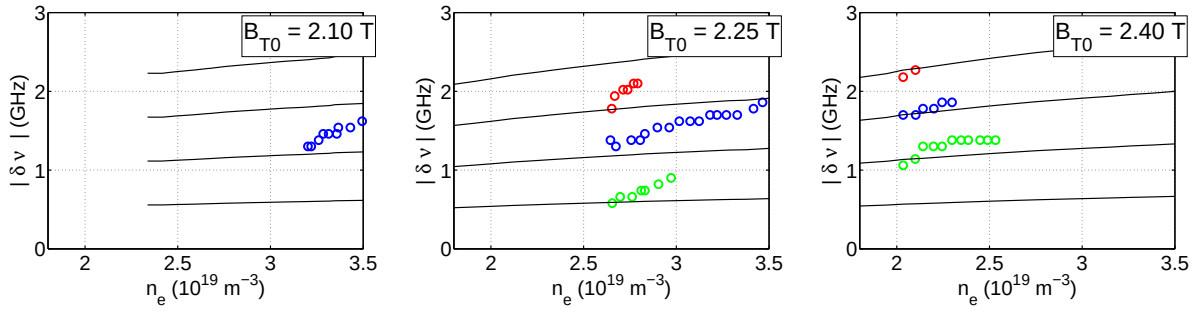


**Figure 12.** End frequencies for frequency chirps during individual island passages as a function of line-averaged electron density. The solid lines represent the first four harmonics of the lower hybrid frequency at the low-field side island position.

## 6. Dependence on the scattering geometry

When the resolved fluctuation wave vector, $\mathbf{k}^{\mathrm{s}} - \mathbf{k}^{\mathrm{i}}$, is close to perpendicular to the magnetic field, the lower hybrid wave, ion Berstein waves and ion cyclotron structures are expected to enter the scattering spectrum [32–37]. Here, $\mathbf{k}^{\mathrm{i}}$ and $\mathbf{k}^{\mathrm{s}}$ refer to the wave vector of the incident and the scattered wave, respectively. The dependence of the strong scattering on the scattering angle and on the angle between $\mathbf{k}^{\mathrm{s}} - \mathbf{k}^{\mathrm{i}}$ and the magnetic field is investigated in the high-density regime by changing the toroidal injection angle of the gyrotron beam. For each gyrotron beam setting the receiver beam pattern was gradually swept toroidally across the gyrotron beam, keeping the overlapping region close to the

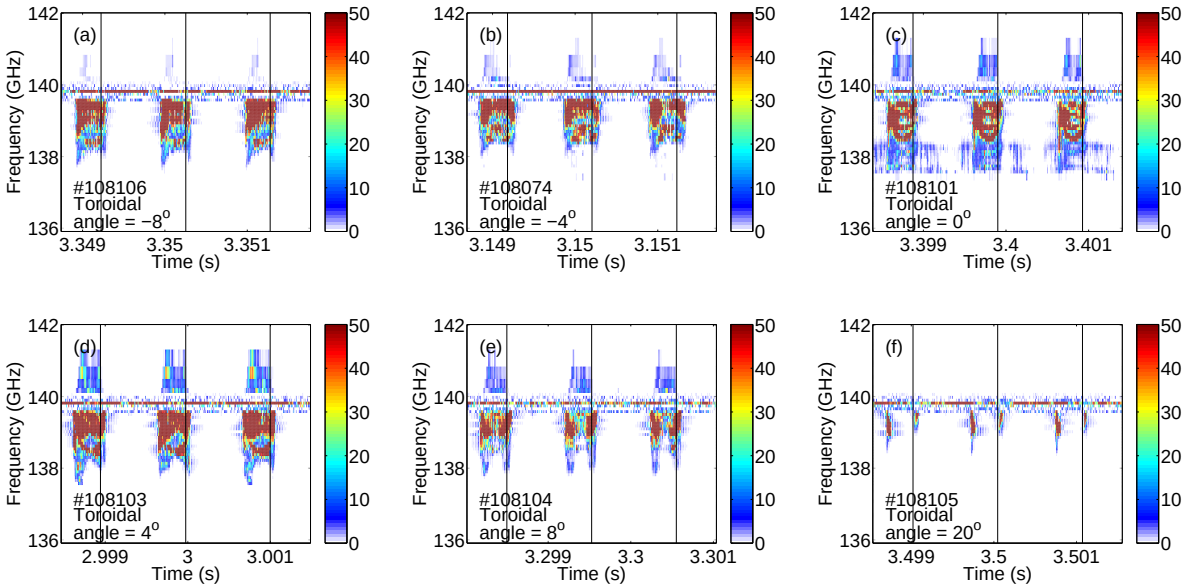


**Figure 13.** Spectral evolution (in MeV) during individual island passages. Discharges with gyrotron toroidal injection angle of (a) -8 , (b) -4, (c) 0, (d) +4, (e) +8, and (f) +20. All discharges have line-averaged densities of $2.55 \pm 0.05 \times 10^{19}$ m $^{-3}$.

island position on the low-field side. The measured spectra at the toroidal receiver angle with highest signal level are shown in figure 13 for gyrotron toroidal injection angles of $-8°, -4°, 0°, 4°, 8°$, and $20°$. These injection angles correspond to an angle between the resolved fluctuation wave vector and the magnetic field, $\phi = \angle(\mathbf{k}^{\mathrm{s}} - \mathbf{k}^{\mathrm{i}}, \mathbf{B})$, of $104°, 99°, 94°, 88°, 83°$, and $65°$, respectively. The scattering angle, $\angle(\mathbf{k}^{\mathrm{i}}, \mathbf{k}^{\mathrm{s}})$, is kept at approximately $140°$ and the line-averaged electron density is $2.55 \pm 0.05 \times 10^{19}$ m $^{-3}$. In this wide range of toroidal injection angle the shape of the scattering signal changes only very little compared to the variation seen for changing density and magnetic field. For a gyrotron injection angle of $20°$ (figure 13f) a slightly reduced level of anomalous scattering is present and no signal is present at the O-point passage time. No data where obtained for gyrotron injection angles of $-20°$.

In dedicated scattering experiments investigating the nature of thermally driven ion Bernstein waves [32–34] and non-thermally driven lower hybrid waves [36–38], the signature of such waves in the scattering spectrum is only present when $\phi$ takes values a few degrees from $90°$. The signals observed for pure radial injection (figure 13c) around 138 GHz could in principle be explained by scattering off non-thermally driven lower hybrid waves (3rd harmonic). However, the majority of the anomalous scattering only has a weak dependence on $\phi$, so it is unlikely that the results can be explained by direct scattering off thermally driven ion Bernstein waves or non-thermally driven lower hybrid waves.

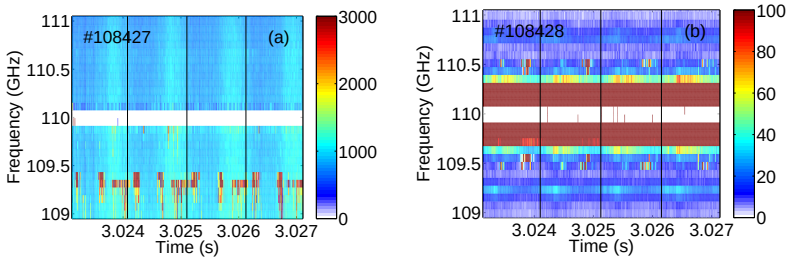


**Figure 14.** Signal during 110 GHz gyrotron operation (in eV). Left: with a resonance deeply inside the plasma. Right: without a resonance in the plasma.

## 7. Strong scattering in the collective Thomson scattering scenario

Lastly, we investigate if strong scattering can occur at a different gyrotron frequency and when the cold electron cyclotron resonances are outside the plasma. We use a 110 GHz gyrotron that normally produced the probe beam in CTS experiments at TEXTOR. First we investigate an ECRH scenario with the cold resonance in the plasma using the 110 GHz gyrotron. For these experiments we set the magnetic field to 1.9 T, the plasma current to 250 kA, and the line-averaged density to $2\times10^{19}$ m $^{-3}$. This scenario is similar to the scenario we investigated using the 140 GHz gyrotron and higher magnetic field and current (discharge #108099 in table 1 and figure 11c). The anomalous scattering is only observed for frequencies below the gyrotron frequency as figure 14 shows, which was also the case for the main part of the data when the 140 GHz gyrotron was used. The upper hybrid frequency was about 70 GHz at the low-field side island position which is larger than half the gyrotron frequency (55 GHz). We therefore suppose that the strong scattering occurs in the high-density regime. This is also supported by a comparison of the spectral shapes in figure 14a with those of figure 9d. The electron density and gyrotron power dependence of the anomalous scattering for 110 GHz gyrotron operation could not be investigated. The nature of the scattering changes significantly in the CTS scenario where the magnetic field is set to 2.6 T so that the resonances are situated just outside the plasma edge. The plasma current was 350 kA to match the q=2 position from previously and the upper hybrid frequency at the low-field side island position was about 90 GHz which is significantly larger than half the gyrotron frequency (55 GHz). In this case bursts of anomalous scattering occur synchronized with the island rotation frequency in particular channels that monitor frequency shifts of about 500 MHz, for frequency up-shift as well as for frequency down-shift. This frequency is typical for the lower hybrid range of frequency, and similar signals have been observed at ASDEX Upgrade [39], at LHD [9], and at Wendelstein 7-AS [37].

## 8. Discussion

The data presented here are not described by current models for collective Thomson scattering that assume thermal fluctuations and homogeneous plasma [40]. The non-

linearity of the received signal with respect to gyrotron power in both the low and high-density regimes indicates that the observations originate from non-linear interaction between the gyrotron radiation and the plasma. A candidate for describing the data is the parametric decay instability (PDI) [18]. In the PDI the main wave decays into a low frequency wave in the MHz to GHz range and a high frequency wave below the gyrotron frequency. In previously reported PDI observations in tokamaks [15], the heating wave decayed into a lower hybrid wave and an electron Bernstein wave. Our measurements suggest that the daughter waves are lower hybrid waves in one of the scattering regimes, and that the scattering is connected with the upper hybrid wave. This supports the hypothesis that PDI could be the main drive of the anomalous scattering. However, we note that whereas previous results have reported the decay to happen near the resonance condition $f_{gyr} = f_{UH}$ [15], we find a modified resonance condition, namely $f_{gyr} = 2 \times f_{UH}$. This result has already inspired theoretical development of PDI models to include a two plasmon decay of upper hybrid waves [21, 31].

In the beginning of the low-density regime, the difference between the gyrotron frequency and the anomalous scattering matches the lower hybrid frequency in the plasma centre. Signals in similar frequency ranges have also been observed in Wendelstein 7-AS during CTS experiments and have been ascribed to lower hybrid turbulence [37] and NBI-driven ion cyclotron instabilities [41]. We here observe a signal which is strongly non-linear with respect to gyrotron power. The fluctuations described in [37] and [41] are in principle independent of the gyrotron power and would be present even without a gyrotron beam. However, in our experiments the different gyrotron power levels also result in different local plasma parameters due to absorption, which could give rise to a non-linear dependence of the instability amplitude on the gyrotron power. So at present an explanation for our data in the low-density regime in terms of lower hybrid turbulence or NBI driven instabilities cannot be ruled out.

Previously, it has been reported that the scattering in the high-density regime is likely to originate from the island position on the low-field side [17]. Since the frequency evolution of the first part of the low-density regime matches the lower hybrid frequency in the plasma centre, we speculate that the scattering in this region originates from the plasma centre. In this hypothesis, when considering the local parameters, the low-density region indicated in figure 5 will move to higher densities and magnetic fields. Then actually the two regimes will occur at similar densities and magnetic fields. We must stress that the location of the scattering signal in the low-density regime has not been verified experimentally. In principle the scattering in the low-density regime could also originate from the island position on the high field side. However, we note that the broadband signal in the end of the low-density regime is rather similar for the 2.1 T and 2.4 T discharges. If the signal originated from the high field side, it should be strongly damped, due to absorption, when the resonance position is placed close to the plasma centre, as is the case for the 2.4 T discharge.

If the anomalous scattering in both the low-density and the high-density regime is explained by parametric decay, one would expect a similar frequency behaviour in the

two regimes. However, in the high-density regime, a strong frequency chirp is observed which is not present in the low-density regime. Whereas signatures of the lower hybrid wave are present in the low-density regime, the picture is less obvious in the high-density regime. At the island position, the local density gradient varies significantly during an island passage, whereas the variation is small in the plasma centre. This difference could in principle give rise to different power thresholds for parametric decay and possible daughter waves which can be exited.

Finally, we note the similarities between our measurements in both the high- and low-density regimes and the reported anomalous signal from the FTU tokamak [42, 43], LHD [9], and at ASDEX Upgrade both in ECRH heated plasmas [44] and during general CTS operation [39] where strong signals are observed in correlation with edge localized modes (ELMs).

## 9. Conclusions

We have characterized anomalous scattering from gyrotron heated TEXTOR plasmas with rotating islands. The signal is strongly dependent on the electron density and the magnetic field. Two regimes of anomalous scattering have been presented which are separated by a quiescent regime. In the low-density anomalous scattering regime the signal carries signatures of the lower hybrid frequency whereas more complex spectra are observed in the high-density regime.

The threshold for the high-density regime is strongly dependent on the magnetic field and the electron density and is connected to the upper hybrid frequency. When the upper hybrid frequency is equal to or slightly above half the gyrotron frequency the anomalous scattering is maximized. The scattering in the high-density regime, which is correlated to the passage of the island O-point through the mm-wave beam [16], is interpreted to originate from the island position on the low-field side. Further, it is speculated that strong anomalous scattering in the low-density regime originates from the plasma centre.

Our results are likely to shed light on the anomalous scattering taking place on ASDEX Upgrade [39, 44], FTU [42, 43] and LHD [9] and to increase the knowledge of parametric decay and scattering off tearing modes. Finally, this might have a bearing for possible CTS operating scenarios on ITER [45].

## Acknowledgments

This work, supported by the European Communities under the contract of Association between EURATOM and DTU, FOM and FZJ, was carried out within the framework of the European Fusion Programme. The views and opinions expressed herein do not necessarily reflect those of the European Commission. The contribution of Egbert Westerhof and Waldo Bongers has been performed in the framework of the NWO-RFBR Centre of Excellence on Fusion Physics and Technology (grant 047.018.002).

## References


[1] Prater R 2004 *Physics of Plasmas* **11** 2349 ISSN 1070664X

[2] Hartfuss H J, Geist T and Hirsch M 1997 *Plasma Physics and Controlled Fusion* **39** 1693–1769 ISSN 0741-3335

[3] Hennen B A, Westerhof E, Nuij P W J M, Oosterbeek J W, de Baar M R, Bongers W A, Bürger A, Thoen D J and Steinbuch M 2010 *Plasma Physics and Controlled Fusion* **52** 104006 ISSN 0741-3335

[4] Oosterbeek J W, Bürger A, Westerhof E, de Baar M R, van den Berg M A, Bongers W A, Graswinckel M F, Hennen B A, Kruijt O G, Thoen J, Heidinger R, Korsholm S B, Leipold F and Nielsen S K 2008 *The Review of scientific instruments* **79** 093503 ISSN 1089-7623

[5] Bongers W A, Goede A P H, Westerhof E, Oosterbeek J W, Doelman N J, Schuller F C, De Baar M R, Kasparek W, Wubie W, Wagner D and Stober J 2009 *FUSION SCIENCE AND TECHNOLOGY* **55** 188–203

[6] Bindslev H, Nielsen S, Porte L, Hoekzema J, Korsholm S, Meo F, Michelsen P, Michelsen S, Oosterbeek J, Tsakadze E, Westerhof E and Woskov P 2006 *Physical Review Letters* **97** 205005 ISSN 0031-9007

[7] Nielsen S, Salewski M, Bindslev H, Bürger A, Furtula V, Kantor M, Korsholm S, Koslowski H, Krämer-Flecken A, Leipold F, Meo F, Michelsen P, Moseev D, Oosterbeek J, Stejner M and Westerhof E 2011 *Nuclear Fusion* **51** 063014 ISSN 0029-5515

[8] Salewski M, Meo F, Stejner M, Asunta O, Bindslev H, Furtula V, Korsholm S, Kurki-Suonio T, Leipold F, Leuterer F, Michelsen P, Moseev D, Nielsen S, Stober J, Tardini G, Wagner D and Woskov P 2010 *Nuclear Fusion* **50** 035012 ISSN 0029-5515

[9] Kubo S, Nishiura M, Tanaka K, Shimozuma T, Yoshimura Y, Igami H, Takahash H, Mutoh T, Tamura N, Tatematsu Y, Saito T, Notake T, Korsholm S B, Meo F, Nielsen S K, Salewski M and Stejner M 2010 *The Review of scientific instruments* **81** 10D535 ISSN 1089-7623

[10] Porkolab M 1978 *Nuclear Fusion* **18** 367–413 ISSN 0029-5515

[11] Erckmann V and Gasparino U 1994 *Plasma Physics and Controlled Fusion* **36** 1869–1962 ISSN 0741-3335

[12] Chang R, Porkolab M and Grek B 1972 *Physical Review Letters* **28** 206–209 ISSN 0031-9007

[13] Okabayashi M, Chen K and Porkolab M 1973 *Physical Review Letters* **31** 1113–1116 ISSN 0031-9007

[14] Bernhardt P A, Selcher C A and Kowtha S 2011 *Geophysical Research Letters* **38** L19107 ISSN 0094-8276

[15] McDermott F S, Bekefi G, Hackett K E, Levine J S and Porkolab M 1982 *Physics of Fluids* **25** 1488 ISSN 00319171

[16] Westerhof E, Nielsen S, Oosterbeek J, Salewski M, De Baar M, Bongers W, Bürger A, Hennen B, Korsholm S, Leipold F, Moseev D, Stejner M and Thoen D 2009 *Physical Review Letters* **103** 125001 ISSN 0031-9007

[17] Nielsen S K, Salewski M, Bongers W, Korsholm S B, Leipold F, Meo F, Michelsen P, Moseev D, Oosterbeek J W, Stejner M and Westerhof E 2012 *The Review of scientific instruments* **83** 113508 ISSN 1089-7623

[18] Gusakov E Z and Popov A Y 2010 *Physical Review Letters* **105** 115003

[19] Gusakov E and Popov A Y 2012 *EPL (Europhysics Letters)* **99** 15001 ISSN 0295-5075

[20] Gusakov E Z and Popov A Y 2010 *JETP Letters* **91** 655–659 ISSN 0021-3640

[21] Gusakov E Z and Popov A 2012 *EPJ Web of Conferences* **32** 01007 ISSN 2100-014X

[22] Gusakov E, Popov A and Saveliev A 2012 *EPJ Web of Conferences* **32** 01002 ISSN 2100-014X

[23] Nielsen S K, Bindslev H, Porte L, Hoekzema J A, Korsholm S B, Leipold F, Meo F, Michelsen P K, Michelsen S, Oosterbeek J W, Tsakadze E L, Van Wassenhove G, Westerhof E and Woskov P 2008 *Physical Review E* **77** 016407 ISSN 1539-3755

[24] Samm U 2005 *Fusion Science and Technology* **47** 73–75 ISSN 1536-1055

[25] Abdullaev S, Finken K, Jakubowski M, Kasilov S, Kobayashi M, Reiser D, Reiter D, Runov A and Wolf R 2003 *Nuclear Fusion* **43** 299–313 ISSN 0029-5515

[26] Koslowski H, Liang Y, Krämer-Flecken A, Löwenbrück K, von Hellermann M, Westerhof E, Wolf R C, Zimmermann O and Team t T 2006 *Nuclear Fusion* **46** L1–L5 ISSN 0029-5515

[27] Westerhof E, Hoekzema J A, Hogeweij G M D, Jaspers R J E, Schuller F C, Barth C J, Bongers W A, Donne A J H, Dumortier P, van der Grift A F, van Gorkom J C, Kalupin D, Koslowski H R, Kramer-Flecken A, Kruijt O G, Cardozo N J L, Mantica P, van der Meiden H J, Merkulov A, Messiaen A, Oosterbeek J W, Oyevaar T, Poelman A J, Polman R W, Prins P R, Scholten J, Sterk A B, Tito C J, Udintsev V S, Unterberg B, Vervier M and Van Wassenhove G 2003 *Nuclear Fusion* **43** 1371–1383 ISSN 0029-5515

[28] Thoen D J, Bongers W A, Westerhof E, Oosterbeek J W, de Baar M R, van den Berg M A, van Beveren V, Bürger A, Goede A P H, Graswinckel M F, Hennen B A and Schüller F C 2009 *The Review of scientific instruments* **80** 103504 ISSN 1089-7623

[29] Koslowski H R and Soltwisch H 1997 *Fusion Engineering and Design* **43** 143–150

[30] Udintsev V S, van de Pol M J, Donne A J H, Oosterbeek J W and Kramer-Flecken A 2001 *Review of Scientific Instruments* **72** 359 ISSN 00346748

[31] Gusakov E Z and Popov A Y 2012 *39th EPS Conference & 16 th Int. Congress on Plasma Physics* p P2.014

[32] Korsholm S B, Stejner M, Bindslev H, Furtula V, Leipold F, Meo F, Michelsen P K, Moseev D, Nielsen S K, Salewski M, de Baar M, Delabie E, Kantor M and Bürger A 2011 *Physical Review Letters* **106** 165004 ISSN 0031-9007

[33] Stejner M, Korsholm S B, Nielsen S K, Salewski M, Bindslev H, Leipold F, Michelsen P K, Meo F, Moseev D, Burger A, Kantor M and de Baar M 2012 *The Review of scientific instruments* **83** 10E307 ISSN 1089-7623

[34] Stejner M, Korsholm S B, Nielsen S K, Salewski M, Bindslev H, Brezinsek S, Furtula V, Leipold F, Michelsen P K, Meo F, Moseev D, Bürger A, Kantor M and de Baar M 2012 *Plasma Physics and Controlled Fusion* **54** 015008 ISSN 0741-3335

[35] Hughes T and Smith S 1988 *Nuclear Fusion* **28** 1451–1457 ISSN 0029-5515

[36] Suvorov E V, Holzhauer E, Kasparek W, Lubyako L V, Burov A B, Dryagin Y A, Fil'chenkov S E, Fraiman A A, Kukin L M, Kostrov A V, Ryndyk D A, Shtanyuk A M, Skalyga N K, Smolyakova O B, Erckmann V, Geist T, Kick M, Laqua H and Rust M 1997 *Plasma Physics and Controlled Fusion* **39** B337–B351 ISSN 0741-3335

[37] Suvorov E, Holzhauer E, Kasparek W, Burov A, Dryagin Y, Fil'chenkov S, Fraiman A, Lubyako L, Ryndyk D, Skalyga N, Smolyakova O, Erckmann V, Geist T, Kick M, Rust N, Team W A and Team E 1998 *Nuclear Fusion* **38** 661–671 ISSN 0029-5515

[38] Suvorov E V, Erckmann V, Holzhauer E, Kasparek W, Dryagin Y A, Fil'chenkov S E, Fraiman A A, Geist T, Kick M, Kukin L M, Kostrov A V, Lubyako L V, Shtanyuk A M, Skalyga N K and Smolyakova O B 1995 *Plasma Physics and Controlled Fusion* **37** 1207–1213 ISSN 0741-3335

[39] Meo F, Stejner M, Salewski M, Bindslev H, Eich T, Furtula V, Korsholm S B, Leuterer F, Leipold F, Michelsen P K, Moseev D, Nielsen S K, Reiter B, Stober J, Wagner D and Woskov P 2010 *Journal of Physics: Conference Series* **227** 012010 ISSN 1742-6596

[40] Bindslev H 1996 *Journal of Atmospheric and Terrestrial Physics* **58** 983

[41] Shalashov A G, Suvorov E V, Lubyako L V, Maassberg H and Team t W A 2003 *Plasma Physics and Controlled Fusion* **45** 395–412 ISSN 0741-3335

[42] Tartari U, Grosso G, Granucci G, Lubyako L, Shalashov A, Suvorov E, Orsitto F, Simonetto A, Nowak S, Volpe F, Bruschi A, Gandini F, Muzzini V, Garavaglia S and Grossetti G 2006 *Nuclear Fusion* **46** 928–940 ISSN 0029-5515

[43] Tartari U, Grosso G, Granucci G, Gandini F, Garavaglia S, Grossetti G, Simonetto A, Mellera V, Muzzini V, Lubyako L, Shalashov A, Orsitto F P, Ciccone G and Volpe F 2007 *The Review of scientific instruments* **78** 043506 ISSN 0034-6748

[44] Bongers W, Kasparek W, Doelman N, van den Braber R, van den Brand H, Meo F, de Baar

M, Amerongen F, Donné A, Elzendoorn B, Erckmann V, Goede A, Giannone L, Grünwald G, Hollman F, Kaas G, Krijger B, Michel G, Lubyako L, Monaco F, Noke F, Petelin M, Plaum B, Purps F, ten Pierik J, Schüller C, Slob J, Stober J, Schütz H, Wagner D, Westerhof E and Ronden D 2012 *EPJ Web of Conferences* **32** 03006 ISSN 2100-014X

[45] Salewski M, Eriksson L G, Bindslev H, Korsholm S, Leipold F, Meo F, Michelsen P and Nielsen S 2009 *Nuclear Fusion* **49** 025006 ISSN 0029-5515